Photoacoustics 41 (2025) 100677

Contents lists available at ScienceDirect

Photoacoustics

journal homepage: www.elsevier.com/locate/pacs

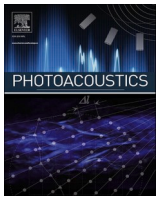

Optomechanical energy enhanced BF-QEPAS for fast and sensitive gas sensing

Weilin Ye [a,b], Linfeng He [a,b], Weihao Liu [a,b], Zhile Yuan [a,b], Kaiyuan Zheng [c,*], Guolin Li [d,*]

[a] Shantou Key Laboratory for Intelligent Equipment and Technology, College of Engineering, Shantou University, 243 Dax-ue Road, Shantou 515063, PR China
[b] Key Laboratory of Intelligent Manufacturing Technology, Ministry of Education, College of Engineering, Shantou University, 243 Daxue Road, Shantou 515063, PR China
[c] Division of Environment and Sustainability, The Hong Kong University of Science and Technology, 999077, Hong Kong
[d] College of Control Science & Engineering, China University of Petroleum (East China), Qingdao 266580, PR China

ARTICLE INFO

Keywords:
Optical sensor
Quartz-enhanced photoacoustic spectroscopy
Continuous beat frequency
Energy accumulation incentive

ABSTRACT

Traditional beat frequency quartz-enhanced photoacoustic spectroscopy (BF-QEPAS) are limited by short energy accumulation times and the necessity of a decay period, leading to weaker signals and longer measurement cycles. Herein, we present a novel optomechanical energy-enhanced (OEE-) BF-QEPAS technique for fast and sensitive gas sensing. Our approach employs periodic pulse-width modulation (PWM) of the laser signal with an optimized duty cycle, maintaining the quartz tuning fork's (QTF) output at a stable steady-state level by applying stimulus signals at each half-period and allowing free vibration in alternate half-periods to minimize energy dissipation. This method enhances optomechanical energy accumulation in the QTF, resulting in an approximate 33-fold increase in response speed and a threefold increase in signal intensity compared to conventional BF-QEPAS. We introduce an energy efficiency coefficient K to quantify the relationship between transient signal amplitude and measurement duration, exploring its dependence on the modulation signal's period and duty cycle. Theoretical analyses and numerical simulations demonstrate that the maximum K occurs at a duty cycle of 50 % and an optimized beat frequency Δf of 30 Hz. Experimental results using methane reveal a detection limit of 2.17 ppm with a rapid response time of 33 ms. The OEE-BF-QEPAS technique exhibits a wide dynamic range with exceptional linearity over five orders of magnitude and a record noise-equivalent normalized absorption (NNEA) coefficient of 9.46×10^{-10} W cm^{-1} Hz$^{-1/2}$. Additionally, a self-calibration method is proposed for correcting resonant frequency shifts. The proposed method holds immense potential for applications requiring fast and precise gas detection.

1. Introduction

Quartz-enhanced photoacoustic spectroscopy (QEPAS) was first reported in 2002 and developed fast in recent years [1–3]. Unlike other gas sensing techniques based on infrared absorption spectroscopy [4–6], such as tunable diode laser absorption spectroscopy (TDLAS) and cavity-enhanced absorption spectroscopy (CEAS), QEPAS utilizes a quartz tuning fork (QTF) as its core detection component [7,8]. This approach offers several advantages, including compact size, low cost, narrow acoustic resonance, and high quality (Q) factor [9–11]. For improve the weak acoustic signal from the gas absorbance, an acoustic micro-resonator (AmR) is usually utilized to realizes strong acoustic coupling between the QTF and the resonant tube [11]. Various structures have been proposed to enhance acoustic coupling strength and improve the gas sensing performance of QEPAS, including the on-beam QEPAS [12], the off-beam QEPAS [13], the embedded off-beam QEPAS [14]. Additionally, customized tuning forks with tailored resonant frequencies can further enhance the signal strength and overall sensor performance, offering improved sensitivity and faster response times for specific applications [15–18].

QEPAS exhibits two primary drawbacks: drift in resonance frequency (f_0) and a slow response speed. Conventionally, the modulation frequency is set to f_0 to maximize the signal amplitude [19,20]. However, f_0 is easily influenced by environmental factors such as pressure, temperature, and gas composition [21–24]. Consequently, frequent calibration of f_0 is necessary during gas sensing operations, leading to discontinuous

* Corresponding authors.
E-mail addresses: kaiyuanzheng@ust.hk (K. Zheng), liguolin@upc.edu.cn (G. Li).

https://doi.org/10.1016/j.pacs.2024.100677
Received 10 November 2024; Received in revised form 3 December 2024; Accepted 5 December 2024
Available online 9 December 2024

monitoring. Moreover, the gradual variation of the continuous acoustic wave induces forced vibrations in the QTF, resulting in response times exceeding 1 s [25]. To address these issues, the beat frequency QEPAS (BF-QEPAS) technique was reported [26]. BF-QEPAS utilizes the transient signal decay time from the tuning fork to quickly determine the resonance frequency. By analyzing the decay time, which is the period it takes for the signal to diminish after the excitation source is turned off, the resonance frequency can be calculated using BF-QEPAS, and the amplitude of the transient signal can also be retrieved as it is proportional to the gas concentration [27–29].

The traditional BF-QEPAS methodology, involving a modulation period followed by a decay phase, is confronted with two primary limitations [30]. The core issue lies in the short energy accumulation time in BF-QEPAS. During the modulation period, the tuning fork is excited, but this excitation is often insufficient to generate a large amplitude response, especially when detecting low concentrations of gases. This limitation results in a weaker acoustic signal, which, when coupled with the ambient noise, adversely affects the signal-to-noise ratio. Moreover, the traditional BF-QEPAS approach necessitates a decay period where the laser signal is turned off, allowing the fork's vibration to decay freely. This phase is crucial for calculating the resonance frequency but results in a longer measurement cycle.

Our research addresses these challenges through the introduction of an innovative optomechanical energy enhance method that capitalizes on the periodic modulation of the laser signal to maintain the tuning fork's output at a stable, steady-state level, often resembling a sinusoidal waveform. This approach departs from the conventional BF-QEPAS decay-based measurement, focusing instead on the steady-state amplitude of the signal. The peak of this sinusoidal waveform correlates with the gas concentration and is influenced by the modulation signal's period and duty cycle (where duty cycle is defined as the ratio of the modulation signal time to the total cycle time). To the best of our knowledge, there have been no prior reports on the utilization of steady-state signal amplitude for gas concentration measurement in the context of BF-QEPAS. Additionally, to provide a comprehensive quantification of transient signal amplitude and measurement duration, we introduce an energy efficiency coefficient K, defined as the ratio between these two parameters. No investigations have hitherto explored the relationship between the efficiency coefficient K and the period as well as the duty cycle of the modulation signal. Furthermore, compared to other advanced gas sensing techniques, such as photoacoustic spectroscopy with MEMS microphones [31] and quartz-enhanced photoacoustic spectroscopy [32], our proposed method offers advantages in terms of response speed and sensitivity. These techniques often involve trade-offs between sensitivity and response time and may require complex setups or high-power lasers. Our optomechanical energy-enhanced BF-QEPAS (OEE-BF-QEPAS) provides a balanced solution with high sensitivity, fast response, and a relatively simple and robust setup.

2. OEE-BF-QEPAS based on steady-state response

2.1. Principle

Fig. 1 illustrates the principle of OEE-BF-QEPAS, which emphasizes the steady-state response enabled by an optimized duty cycle of pulse-width modulation (PWM). As shown in Fig. 1(a), the generation of laser light involves overlaying a direct current (DC) signal for adjusting the laser to the absorption line, along with a sine wave for modulating the QTF (Eq. 1). The key to enhancing energy efficiency lies in the PWM, which is represented by a duty cycle of t_1/T that will be further optimized as discussed in subsequent section to ensure the energy accumulation in the QTF.

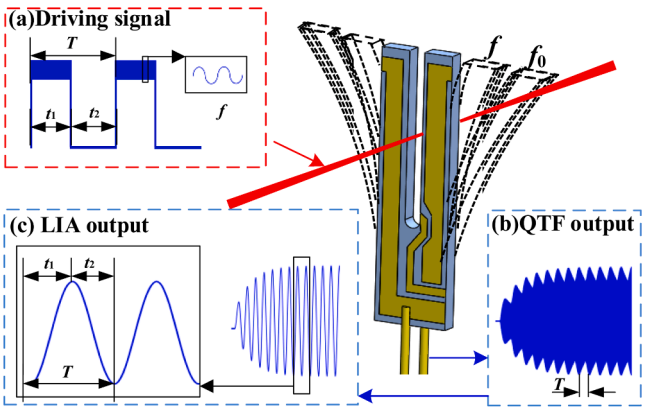

Fig. 1. The principal schematic of OEE-BF-QEPAS.

The modulated light beam passes through the gas mixture and enters the gap of the QTF, as the system operates within the designed driving period T and sine frequency f. When encountering target molecules like methane (CH_4) or carbon dioxide (CO_2), specific wavelengths of the light are absorbed (Eq. 2), causing the molecules to transition energetically and subsequently release heat during relaxation. The resultant heat produces pressure waves in the photoacoustic cell, which in turn generate sound waves (Eq. 3), prompting the QTF to vibrate (Eq. 4). The QTF's vibrations, at a beat frequency offset by Δf from its resonance frequency, result in the generation of an electrical signal via the piezoelectric effect (Eq. 5), as illustrated in Fig. 1(b).

This signal is subsequently processed by a lock-in amplifier (LIA), detailed in Fig. 1(c). The LIA, synchronized to the beat frequency, filters out noise by only amplifying signals at the reference frequency. In the last phase of the PWM cycle (t_2), there is an absence of the driving signal, allowing the QTF to resonate freely at its natural frequency. This resonant signal is fed into the LIA, mixed with a reference signal set at the beat frequency. This mixing process produces a signal containing components at both the sum and difference of the input and reference frequencies. A low-pass filter within the LIA isolates the difference frequency component, effectively extracting a signal with a period of T. By optimizing system parameters, including the beat frequency and duty cycle, the apparatus sustains a steady-state response while optimizing energy efficiency.

The vibration characteristics of the QTF can be effectively analyzed using the classical spring oscillator model, as expressed by Eqs. (1)–(5) [19]:

$$I_0 = \begin{cases} \eta_{EO}(A\sin(\omega t) + B), (0 < t < t_1) \\ 0, (t_1 < t < T) \end{cases} \tag{1}$$

$$I = I_0[1 - \exp(-\alpha CL)] \tag{2}$$

$$F = \eta_{PA} I \tag{3}$$

$$M\frac{d^2x}{dt^2} + c\frac{dx}{dt} + kx = F_0\sin(\omega t) \tag{4}$$

$$U_{QTF}(t) = \eta_{PO} X(t) \tag{5}$$

Here, I_0 (unit: W/m^2) is the emission light intensity, $\eta_{EO}$is the electro-optical conversion coefficient, A and B are the amplitude of sine and DC

signals respectively, T (unit: s) is the square wave period, I is the light intensity reaching the QTF after absorption by the target gas, α(unit: cm^{-1}) is the absorption coefficient, C (unit: ppm) is the concentration of the target gas, L (unit: m) is the optical length, F (unit: μN) is the external force acting on the QTF, η_{PA} is the photoacoustic conversion coefficient, M (unit: μg) represents the total mass of the QTF prongs, x (unit: μm) represents the transverse displacement of the QTF, c (unit: $\mu g.s^{-1}$) denotes the damping coefficient that characterizes the rate of energy dissipation during QTF vibration, and k (unit: $\mu N.\mu m^{-1}$) is the elastic modulus of the QTF material. Since the vibration of the QTF prongs involves small displacement, k can be assumed to be constant, and the stress produced by its deformation is linear. $U_{QTF}(t)$(unit: mV) is the output voltage of QTF, η_{PO} is the piezoelectricity conversion coefficient, and $X(t)$ (unit: μm) is the general solution of Eq. (4) which can be express as follow:

$$X(t) = A_1 e^{-\xi\omega_n t}\sin(\omega_t t+\varphi_1) + F_0A_2\sin(\omega t+\varphi_2) + F_0A_3 e^{-\xi\omega_n t}\sin(\omega_t t+\varphi_3) = C\cos(\omega_t t+\varphi) + F_0A_2\sin(\omega t+\varphi_2) \quad (6)$$

In this equation, $C=\sqrt{A_1^2+F_0^2A_2^2}e^{-\xi\omega_n t}$ and $\varphi=\arctan(F_0A_3/A_1)$ (unit: rad) determine the amplitude and phase of the vibration, respectively. Then $U_{QTF}(t)$ passes the LIA with the reference signal $D\sin(\omega t+\varphi_4)$, and after low-pass filtering, the high-frequency and DC components are filtered out, and the output signal $U_{QTF}(t)$ can be represented as:

$$U_{QTF}(t) = K_1\sin[(\omega_t-\omega)t+\varphi_5] \quad (7)$$

In which, $K_1=\eta_{PO}CD/2$ and $\varphi_5=\varphi-\varphi_4$. Furthermore, the difference between resonant frequency f_0 and beat frequency f(unit: Hz) can be defined as $\Delta f=|f_0-f|$. Then $\omega_t-\omega=2\pi(f_0-f)=2\pi\Delta f=2\pi/T$, hence the period T of the square wave is determined by the value Δf, with adjustments made to T to correspond to varying values of Δf. The Eq. (7) can be expressed as:

$$U_{QTF}(t) = K_1\sin[2\pi t\Delta f+\varphi_5] = K_1\sin[2\pi t/T+\varphi_5] \quad (8)$$

To assess the energy efficiency of QTF, we introduce an energy efficiency coefficient K, which reflects the energy accumulated by QTF within a single cycle time, factoring in the maximum output signal:

$$K = U_{QTF}(t)/T \quad (9)$$

2.2. Optomechanical energy enhanced efficiency study

As shown in Fig. 2, MATLAB calculations were conducted to study the QTF's energy enhancement processor under various patterns. Three distinct stimulation signals, illustrated in Fig. 2(a), were employed: intermittent stimulation, short-term stimulation and continuous stimulation. It can be clearly seen that Y component of the 1 f signals $U_{tY}(t)$ in our technique is much larger than in the others, reflecting the QTF's mechanical vibration. Fig. 2(b) shows the detail of the stimulus signal U_{Drive} used to drive the laser as per Eq. (1), and the Y components of the first harmonic (1 f) signal $U_{tY}(t)$, which reflect the QTF vibration, as well as the R components of 1 f signal $U_{tR}(t)$, representing the energy accumulation. The specific QTF energy analysis is elucidated as follows:

For BF-QEPAS, during the stimulating period of t_1, the QTF experiences forced vibration, involving both transient and steady-state responses. After the stimulus stops, initiating damp free vibration, the QTF undergoes a gradual reduction in vibration amplitude. Fig. 2(a) and (b) showcases the QTF energy, where the amplitude is solely associated with QTF displacement, equating to elastic potential energy accumulated during the t_1 interval. Subsequent to the cessation of stimulation, the QTF undergoes free vibration with damping in the ambient environment and will gradually lose energy. If t_2 is long enough, it would approach zero, which is the ring-down process in the traditional BF-QEPAS. However, if t_2 is selected appropriately, it would stabilize at a fixed value.

We define the period during which energy peaks as the "peak effect" and the subsequent decline as the "valley effect". To enhance the energy efficiency, the duty cycle of the stimulus signal should be studied and optimized. Fig. 2(c) shows the $U_{tY}(t)$ signal under different duty cycles and Fig. 2(d) is the specific signal details under the duty cycles of 25 %,

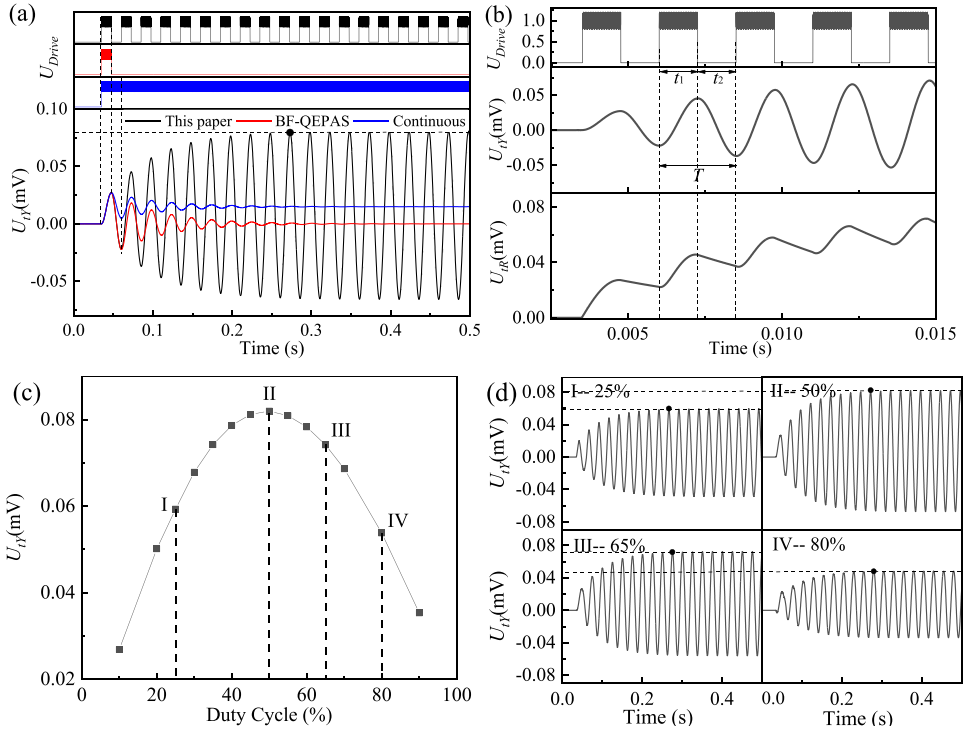

Fig. 2. (a) Corresponding 1 f signals under different QEPAS techniques; (b) the driving signal and the Y and R components of the 1 f signal; (c) stimulation signals under different duty cycles; and (d) specific signal details under duty cycles of 25 %, 50 %, 65 % and 80 %.

50 %, 65 % and 80 %. With the increasing duty cycle from 10 %, the signal rises, reaches the maximum value at 50 %, and then decreases. This simulation result is consistent with theoretical calculation of Eqs. (6)–(8) in Section 2.1. The output signal $U_{QTF}(t)$ is positive in every first half-cycle $T/2 = 1/2\Delta f = 1/2(\omega_t - \omega_s)$, representing the accumulation of energy, and negative in each latter half-cycle, representing the consumption of energy.

The mechanism of these effects can be explained as following: The vibration frequencies caused by the transient response and steady-state response on the QTF are ω_t and ω_s, respectively, with the same initial phase and vibration direction. These vibrations combine on the QTF, resulting in energy augmentation at the outset (t_1). However, due to frequency disparities, the phase differences accumulate and reach a maximum of 180° after the period of $T/2$, coinciding with peak energy, termed the "peak effect". Energy begins to diminish as a consequence of antiparallel phase responses during the period (t_2), reaching a minimum and constituting the "valley effect". The valley effect is discernible as energy loss owing to opposing phases of free and forced vibrations.

Based on the above-mentioned energy analyses, an OEE-BF-QEPAS method is proposed to achieve the maximum QTF energy. Stimulus signals are administered during the peak effect stage to accumulate energy, whereas during the valley effect stage, stimulation is halted to facilitate free vibration, thereby reducing energy dissipation. Energy accumulates from one cycle to the next, ultimately reaching a dynamic equilibrium state, culminating in maximal energy efficiency. Furthermore, after 10 cycles of equipment startup, both simulations and experiments indicate that the signal attains a dynamic equilibrium state.

2.3. Energy efficiency coefficient

For further comparison between traditional BF-QEPAS and our OEE-BF-QEPAS, and to optimize the system parameters, simulation calculations were conducted. Fig. 3 displays the energy efficiency coefficient K for both BF-QEPAS and OEE-BF-QEPAS across varying incentive duty cycles. The outcomes consistently validate the earlier analysis, showing that the maximum K occurs at a duty cycle of 50 %, surpassing that of BF-QEPAS by ~2 orders of magnitude.

2.4. Resonant frequency self-calibration fitting

As shown in Fig. 3, to achieve maximum energy efficiency, there is no ring-down process in OEE-BF-QEPAS. However, the resonant frequency of the QTF may shift due to certain disturbances. To address this shift, a self-calibration method was introduced into the system. As shown in Fig. 2(b), the decrease in each period t_2 of X_{tY}, under the initial beat frequency (f_{int}), can be extended by the free decay of $A_{XtY}e^{-a(x+b)}\cos(2\pi\Delta f + \varphi)$, where A_{XtY} represents the amplitude of the LIA output signal X_{tY}. Each t_2 period of X_{tY} (black line) can be obtained, and parameters of a, b and Δf can be calculated based on the above formula, which is shown as the red line in Fig. 4(a). In this case, $f_0 = f_{\text{int}} + \Delta f = 32751.08$ Hz can be calibrated which is close to the measurement result depicted in Fig. 4(b), as well as the frequency response value of QTF shown in Fig. 6(b).

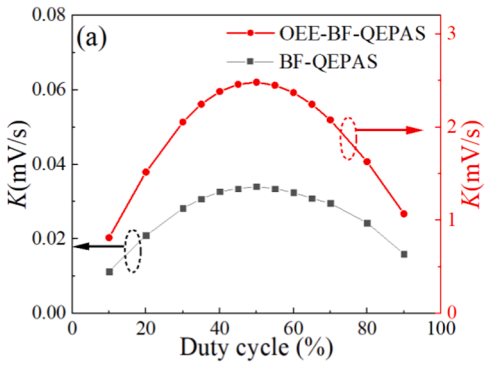

Fig. 3. Comparison of energy efficiency coefficient in OEE-BF-QEPAS and BF-QEPAS under different duty cycles.

3. Sensor structure and performance

3.1. Sensor structure

The architecture of the OEE-BF-QEPAS system is meticulously illustrated in Fig. 5, encompassing both its photoelectric and mechanical components. Within the photoelectric segment, a distributed feedback (DFB) laser is used as the excitation source, with a selected wavelength of 1653 nm corresponding to a prominent near-infrared absorption line characteristic of methane (CH_4), as shown in the bottom right corner of Fig. 5. The DFB laser's temperature and current are controlled by an integrated laser driver (LDTC 0520). A DFB wavelength of 1653 nm is achieved with a temperature of 31 °C and a driver current of 85 mA. The modulation frequency applied to the laser is generated using a LabVIEW program housed in a dedicated computer (PC) and subsequently transmitted through a data acquisition (DAQ) card (NI USB-6361). The DAQ card additionally facilitates real-time monitoring of the DFB laser's temperature and current, providing these essential parameters within the LabVIEW program for continuous tracking. In addition, the QTF piezoelectric signal is amplified using a transimpedance amplifier, which is subsequently subjected to a lock-in amplifier with an integration time of 3 ms, and is transferred to the LabVIEW program through the DAQ card, ultimately being converted into concentration values. As shown in the upper right corner of Fig. 5, the mechanical aspects of the system encompass a QTF, two tubes for coupling QTF vibration, and a specialized cell fabricated by 3D printing process.

3.2. Optimization of parameters

The experimental optimization of wavelength modulation depths for the OEE-BF-QEPAS systems is elucidated in Fig. 6(a). The optimization is based on K measurements at a CH_4 concentration of 5000 ppm. The figure showcases K at $\Delta f = 30$ Hz and laser modulation currents ranging from 0 to 30 mA. The maximum K was consistently achieved at a modulation current of 12 mA, which was selected for subsequent experiments. The frequency response of the QTF, obtained by scanning around the resonance frequency f_0=32750.7 Hz, is shown in Fig. 6(b), and the corresponding K across various frequencies are presented as well. Values of Δf larger and smaller than f_0 exhibit similar trends, but this energy accumulation does not exhibit continual growth; instead, it attains a maximum value and then slightly decreases. In our experiment setup, an optimal $|\Delta f|$ of 30 Hz was determined, which corresponds to a period T of 33 ms based on Eq. (8). This period also represents the system's response time, as it encompasses a full cycle of energy accumulation and dissipation, reflecting the system's ability to stabilize and reach dynamic equilibrium.

3.3. System calibration

To investigate the detection range of OEE-BF-QEPAS, CH_4 cylinders with concentrations of 5000 ppm (low concentration) and 10 % (high concentration) were utilized and diluted with pure N_2 for sensor performance evaluation. Six CH_4 samples with concentrations of 0, 1000, 2000, 3000, 4000 and 5000 ppm were prepared and introduced into the photoacoustic detection cell at a flow rate of 100 sccm. The energy efficiency coefficient K and the corresponding fitting curve are presented in Fig. 7(a), which exhibits high linearity with an R^2 value of 0.99919. Additionally, CH_4 samples with high concentrations of 0.5 %, 2 %, 4 %, 6 %, 8 %, and 10 % were introduced into the cell individually. The correlation between concentration and K is depicted in Fig. 7(b), demonstrating a good linear relationship with an R^2 value of 0.99314.

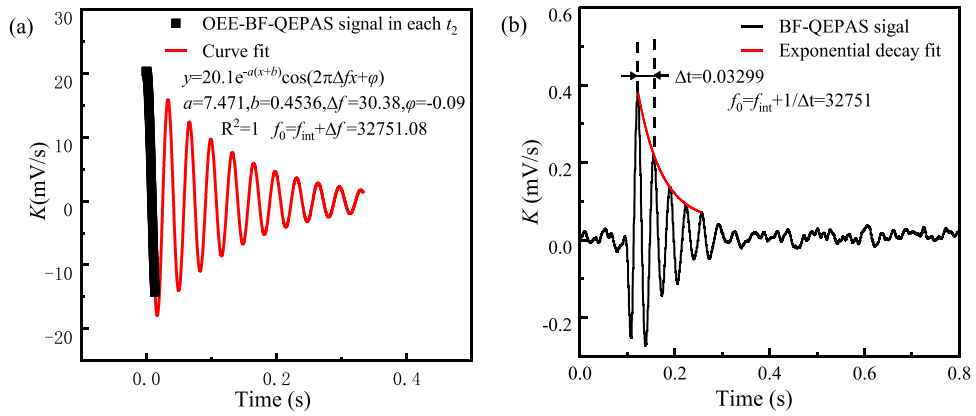

Fig. 4. (a) One t_2 period of X_{tY} (black line) for resonant frequency self-calibration fitting (red line) and (b) the measured one under the CH_4 concentration level of 5000 ppm.

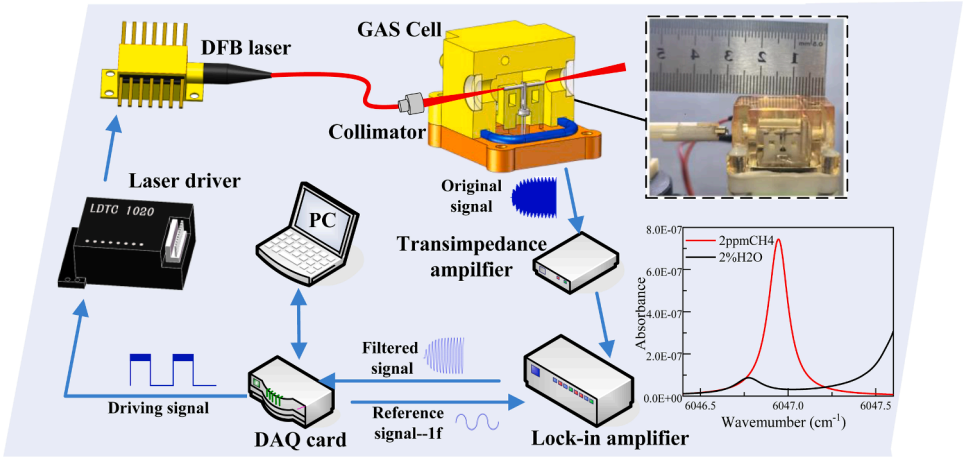

Fig. 5. Schematic of the OEE-BF-QEPAS system. Inset shows the mechanical aspects of the system and the near-infrared absorption line of CH_4.

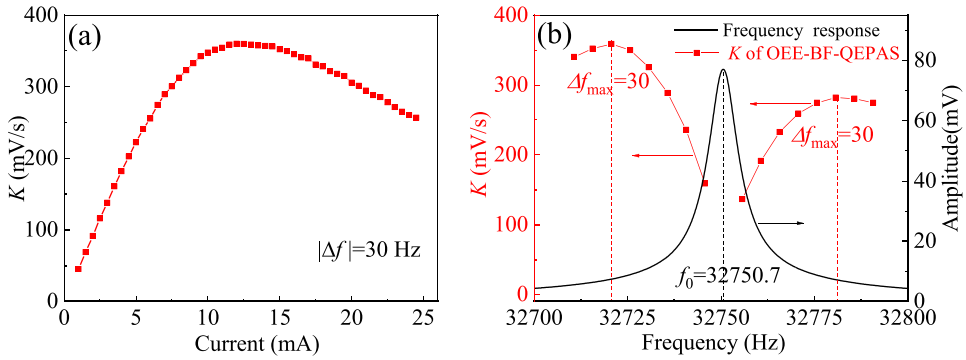

Fig. 6. (a) Modulation depth of energy efficiency coefficient K at Δf of 30 Hz, (b) K *under* the frequency response of QTF.

3.4. Detection limit

To study the detection limit and responding time of OEE-BF-QEPAS, experiments were carried out under a constant CH_4 concentration of 5000 ppm. Fig. 8(a) shows the experimental data over 300 s, and Fig. 8 (b) illustrates the Allan-Werle deviations as a function of the averaging time (τ). The detection limits initially decrease and then increase, reaching a minimum of 2.17 ppm at 25.3 s for OEE-BF-QEPAS. Experimental results have demonstrated good performance of this sensor, particularly in terms of its linearity at lower detection limits and quicker response times compared to traditional QEPAS techniques.

3.5. Self-calibration and correction of resonant frequency shift

When a QTF is exposed to the atmosphere, the presence of airborne dust particles and environmental variations will influence the resonant frequency, consequently impacting the accuracy of the final detection outcome. As illustrated in Fig. 9(a), experiments conducted at a methane concentration of 5000 ppm revealed an initial resonant frequency of 32750.7 Hz and a beat frequency of 32720.7 Hz. Subsequently, after a period of two months without recalibration, an uncorrected shift in the resonant frequency was observed, leading to a change in the detected concentration from 5062 ppm to 3861 ppm. Based on the self-

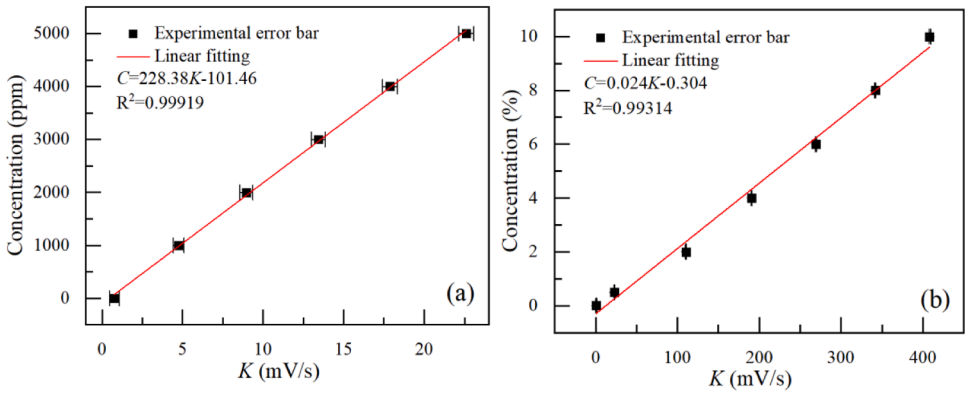

Fig. 7. Experimental data and fitting curve depicting the relationship between CH_4 concentration and energy efficiency coefficient K under (a) low and (b) high concentrations.

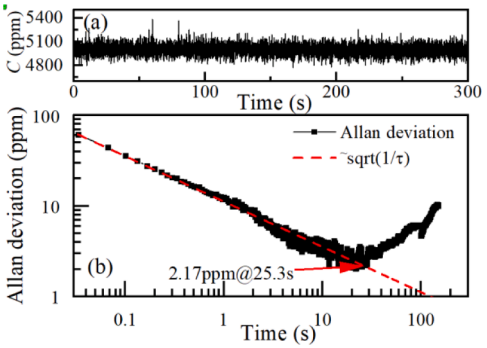

Fig. 8. (a) Long-term measurement of OEE-BF-QEPAS in 5000 ppm CH_4, (b) Allan deviation.

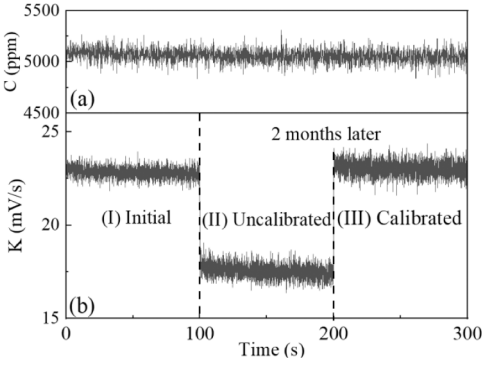

Fig. 9. (a) Concentration of CH_4 in the system, the detection results of (I) initialf_0 = 32750.7Hz, (II) after two months without calibration, f_0 = 32748.45 Hz and (III) calibrated results.

calibration method in Section 2.4, the calculated Δf of 27.75 Hz, shifting the resonant frequency to 32748.45 Hz. Based on the self-calibration parameters, the ideal Δf was determined to be 30 Hz, resulting in a beat frequency change to 32718.45 Hz. The third section of Fig. 9(b) demonstrates the successful calibration of the detection results.

4. Comparison

4.1. Comparison between BF-QEPAS and OEE-BF-QEPAS

To compare the performance differences between the BF-QEPAS and OEE-BF-QEPAS techniques We carried out experiments under the same system using BF-QEPAS. In the BF-QEPAS technique, a sawtooth wave with modulation currents ranging from 75 to 95 mA was employed to drive the DFB laser. To capture the complete exponentially damped oscillation process of the beat frequency signal, the beat frequency period was set to 0.8 s with a duty cycle of 12.5 %. More detailed principles underlying the BF-QEPAS driving mechanism are discussed in Ref. [30]. Fig. 10 (a) demonstrates the calibration of the BF-QEPAS and our OEE-BF-QEPAS techniques. Pure N_2 and five CH_4 samples with concentrations of 1000, 2000, 3000, 4000, and 5000 ppm were prepared, and the resulting output signals were recorded. Both the BF and our OEE-BF methods exhibit excellent linearity, with the OEE-BF energy efficiency coefficient consistently surpassing the BF-QEPAS output at each concentration level. As both techniques utilize the same detection system, the system noise remains constant. Consequently, our OEE-BF-QEPAS technique exhibits a higher signal-to-noise ratio.

To compare the detection limit of two techniques, experiments were carried out under a constant CH_4 concentration of 5000 ppm. Fig. 10(b) illustrates the Allan-Werle deviations as a function of the averaging time (τ) for both methods. The detection limits reach a minimum of 2.17 ppm at 25.3 s for our OEE-BF-QEPAS and 10.27 ppm at 184 s for BF-QEPAS. Furthermore, under the same averaging time of 2.4 s, the Allan deviation for OEE-BF-QEPAS is 7.15 ppm, significantly lower than the 88.06 ppm observed for BF-QEPAS. These results underscore the fast response and high sensitivity of our OEE-BF-QEPAS technique for monitoring gas molecules.

4.2. Comparison between OEE-BF-QEPAS and other QEPAS sensors

Table 1 provides a comprehensive comparison of the performances of several QEPAS-based gas sensors, including the reported QEPAS [32], BF-QEPAS [30], and our proposed OEE-BF-QEPAS, all operating in the near-infrared range and targeting CH_4 with the same absorption line. It can be clearly seen that the developed OEE-BF-QEPAS demonstrates the shortest integration time of only 3 ms and a fast response time of 33 ms, respectively. A fast response time may facilitate more averaging in the same sampling period (e.g., 1 Hz), which can effectively reduce the Gaussian noise level, and thereby improving the signal-to-noise ratio and the overall sensing performance. Furthermore, using the same optical system, the noise-equivalent normalized absorption (NNEA) of our OEE-EB-QEPAS is determined to be 9.46×10^{-10} cm^{-1} W $Hz^{-1/2}$, which represents an approximately one order of magnitude improvement over BF-QEPAS and nearly two orders over traditional QEPAS.

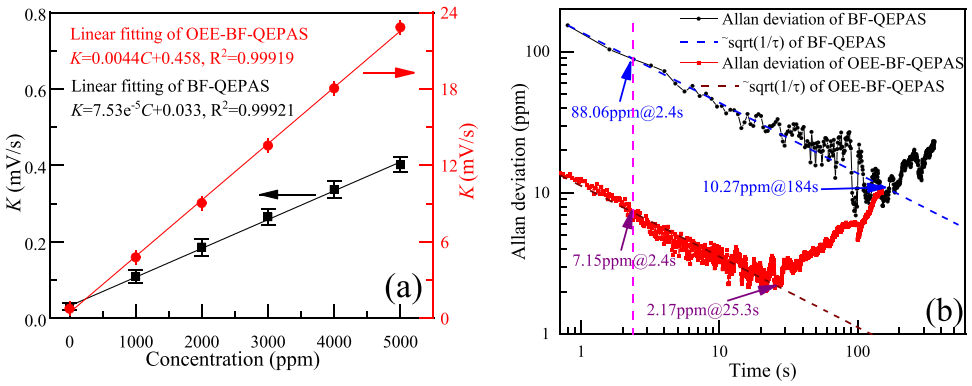

Fig. 10. (a) Calibration of BF-QEPAS and OEE-BF-QEPAS techniques under six different concentrations, (b) Allan deviation of BF-QEPAS and OEE-BF-QEPAS techniques.

Table 1
Performance comparison among QEPAS, BF-QEPAS, and OEE-BF-QEPAS for CH_4 detection.

Technique	Laser type	Wavenumber (cm^{-1})	Integration time (ms)	LoD (ppm)	NNEA (cm^{-1} W $Hz^{-1/2}$)	Response time (s)
QEPAS[32]	DFB-DL	6046.95	1000	0.288	7.76×10^{-8}	1
BF-QEPAS[30]	DFB-DL	6046.95	10	28.35	1.93×10^{-9}	1
BF-QEPAS (this system)	DFB-DL	6046.95	3	10.27	9.44×10^{-9}	0.8
OEE-BF-QEPAS (this work)	DFB-DL	6046.95	3	2.17	9.46×10^{-10}	0.033

5. Conclusion

In this work, we proposed a novel approach for fast-response and high-sensitivity gas molecule (CH_4) sensing through optomechanical energy-enhanced BF-QEPAS technique. Our approach systematically incorporates the QTF vibration module, theoretical analysis of energy accumulation, and the construction of a comprehensive system to facilitate a comparison and optimization of parameters for both conventional BF-QEPAS and OEE-BF-QEPAS techniques. The results from these comparative experiments demonstrate the capabilities of OEE-BF-QEPAS, with a fast response time of 33 ms, in contrast to the approximately 1 s of BF-QEPAS. Moreover, the OEE-BF-QEPAS technique achieves a CH_4 detection sensitivity of 2.17 ppm, whereas BF-QEPAS demonstrates a sensitivity of 10.27 ppm. Calibration experiments have revealed the sensor's wide dynamic range, covering CH_4 concentrations from 0 % to 10 %, characterized by exceptional linearity over five orders of magnitude. The obtained NNEA coefficient of 9.46×10^{-10} cm^{-1} W $Hz^{-1/2}$ underscores the high sensitivity of this technique. The proposed novel OEE-BF-QEPAS technique exhibits immense potential for applications demanding fast and precise gas detection, especially for the monitoring of gas molecules, thus addressing the increasing need for highly responsive and sensitive sensing solutions.

CRediT authorship contribution statement

Guolin Li: Supervision, Funding acquisition. **Kaiyuan Zheng:** Writing – review & editing, Supervision. **Zhile Yuan:** Resources, Data curation. **Weihao Liu:** Methodology. **Linfeng He:** Data curation. **Weilin Ye:** Writing – original draft, Supervision.

Declaration of Competing Interest

The authors declare that they have no known competing financial interests or personal relationships that could have appeared to influence the work reported in this paper.

Acknowledgements

The authors acknowledge the financial support of the National Natural Science Foundation of China (Grant No. 62475139), the Guangdong Basic and Applied Basic Research Foundation (No. 2022A1515011359), the Science and Technology Planning Project of Guangdong Province (Nos. STKJ2021131, DZX_053).

Data availability

Data will be made available on request.

References

[1] A.A. Kosterev, Yu.A. Bakhirkin, R.F. Curl, F.K. Tittel, Quartz-enhanced photoacoustic spectroscopy, Opt. Lett. 27 (2002) 1902, https://doi.org/10.1364/OL.27.001902.
[2] G. Felizzato, N. Liberatore, S. Mengali, R. Viola, V. Moriggia, F.S. Romolo, A deep learning approach to investigating clandestine laboratories using a GC-QEPAS sensor, Chemosensors 12 (2024) 152, https://doi.org/10.3390/chemosensors12080152.
[3] G. Menduni, A. Zifarelli, E. Kniazeva, S.D. Russo, A.C. Ranieri, E. Ranieri, P. Patimisco, A. Sampaolo, M. Giglio, F. Manassero, E. Dinuccio, G. Provolo, H. Wu, L. Dong, V. Spagnolo, Measurement of methane, nitrous oxide and ammonia in atmosphere with a compact quartz-enhanced photoacoustic sensor, Sens. Actuators B: Chem. 375 (2023) 132953, https://doi.org/10.1016/j.snb.2022.132953.
[4] T. Strahl, J. Steinebrunner, C. Weber, J. Wollenstein, K. Schmitt, Photoacoustic methane detection inside a MEMS microphone, Photoacoustics 29 (2023) 100428, https://doi.org/10.1016/j.pacs.2022.100428.
[5] L. Fu, P. Lu, C. Sima, J. Zhao, Y. Pan, T. Li, X. Zhang, D. Liu, Small-volume highly-sensitive all-optical gas sensor using non-resonant photoacoustic spectroscopy with dual silicon cantilever optical microphones, Photoacoustics 27 (2022) 100382, https://doi.org/10.1016/j.pacs.2022.100382.
[6] H. Xiao, J. Zhao, C. Sima, P. Lu, Y. Long, Y. Ai, W. Zhang, Y. Pan, J. Zhang, D. Liu, Ultra-sensitive ppb-level methane detection based on NIR all-optical photoacoustic spectroscopy by using differential fiber-optic microphones with gold-chromium composite nanomembrane, Photoacoustics 26 (2022) 100353, https://doi.org/10.1016/j.pacs.2022.100353.
[7] S. Qiao, Y. He, H. Sun, P. Patimisco, A. Sampaolo, V. Spagnolo, Y. Ma, Ultra-highly sensitive dual gases detection based on photoacoustic spectroscopy by exploiting a

long-wave, high-power, wide-tunable, single-longitudinal-mode solid-state laser, Light-Sci. Appl. 13 (2024) 100, https://doi.org/10.1038/s41377-024-01459-5.
[8] H. Lin, H. Zheng, B.A.Z. Montano, H. Wu, M. Giglio, A. Sampaolo, P. Patimisco, W. Zhu, Y. Zhong, L. Dong, R. Kan, J. Yu, V. Spagnolo, Ppb-level gas detection using on-beam quartz-enhanced photoacoustic spectroscopy based on a 28 kHz tuning fork, Photoacoustics 25 (2022) 100321, https://doi.org/10.1016/j.pacs.2021.100321.
[9] D. Pinto, H. Moser, J.P. Waclawek, S. Dello Russo, P. Patimisco, V. Spagnolo, B. Lendl, Parts-per-billion detection of carbon monoxide: a comparison between quartz-enhanced photoacoustic and photothermal spectroscopy, Photoacoustics 22 (2021) 100244, https://doi.org/10.1016/j.pacs.2021.100244.
[10] R. Rousseau, D. Ayache, N. Maurin, W. Trzpil, M. Bahriz, A. Vicet, Monolithic double resonator for quartz enhanced photoacoustic spectroscopy, Appl. Sci. 11 (2021) 2094, https://doi.org/10.3390/app11052094.
[11] Z. Wang, C. Tian, S. Qian, Y. Yu, J. Chang, Q. Zhang, Y. Feng, H. Li, Z. Feng, A comprehensive dual-spectroscopy detection technique based on TDLAS and QEPAS using a quartz tuning fork, Opt. Laser Technol. 145 (2022) 107483, https://doi.org/10.1016/j.optlastec.2021.107483.
[12] F. Wang, J. Chang, Q. Zhang, Z. Qin, C. Zhu, Pivotal techniques evaluation in QEPAS system for engineering applications, Measurement 135 (2019) 376–384, https://doi.org/10.1016/j.measurement.2018.11.060.
[13] R. Rousseau, Z. Loghmari, M. Bahriz, K. Chamassi, R. Teissier, A.N. Baranov, A. Vicet, Off-beam QEPAS sensor using an 11-μm DFB-QCL with an optimized acoustic resonator, Opt. Express 27 (2019) 7435, https://doi.org/10.1364/OE.27.007435.
[14] L. Qin, S. Bi, R. Chen, Y. Zhao, J. Shi, H. Zhang, Z. Wang, Two-Component Gas Sensor of Time-Division Multiplexing Technique Based on QEPAS and LITES, IEEE Photon. Technol. Lett. 36 (2024) 1085–1088, https://doi.org/10.1109/LPT.2024.3435733.
[15] Y. Liu, S. Qiao, C. Fang, Y. He, H. Sun, J. Liu, Y. Ma, A highly sensitive LITES sensor based on a multi-pass cell with dense spot pattern and a novel quartz tuning fork with low frequency, 230230–230230, Opto-Electron. Adv. 7 (2024), https://doi.org/10.29026/oea.2024.230230.
[16] Y. Ma, S. Qiao, R. Wang, Y. He, C. Fang, T. Liang, A novel tapered quartz tuning fork-based laser spectroscopy sensing, Appl. Phys. Rev. 11 (2024) 41412, https://doi.org/10.1063/5.0214874.
[17] Y. Ma, Y. Liu, Y. He, S. Qiao, H. Sun, Design of multipass cell with dense spot patterns and its performance in a light-induced thermoelastic spectroscopy-based methane sensor, Light: Adv. Manuf. 6 (1) (2025), https://doi.org/10.37188/lam.2025.001.
[18] H. Sun, S. Qiao, Y. He, Y. Liu, Y. Ma, Highly sensitive CH4, C2H2 and CO simultaneous measurement LITES sensor based on multi-pass cell with overlapped spots pattern and QTFs with low resonant frequency, Opt. Express 32 (2024) 28183, https://doi.org/10.1364/OE.531925.
[19] S. Li, Y. Yuan, Z. Shang, X. Yin, A. Sampaolo, P. Patimisco, V. Spagnolo, L. Dong, H. Wu, Ppb-level NH3 photoacoustic sensor combining a hammer-shaped tuning fork and a 9.55 μm quantum cascade laser, Photoacoustics 33 (2023) 100557, https://doi.org/10.1016/j.pacs.2023.100557.
[20] B. Li, G. Menduni, M. Giglio, P. Patimisco, A. Sampaolo, A. Zifarelli, H. Wu, T. Wei, V. Spagnolo, L. Dong, Quartz-enhanced photoacoustic spectroscopy (QEPAS) and beat frequency-QEPAS techniques for air pollutants detection: a comparison in terms of sensitivity and acquisition time, Photoacoustics 31 (2023) 100479, https://doi.org/10.1016/j.pacs.2023.100479.
[21] V. Spagnolo, P. Patimisco, S. Borri, A. Sampaolo, G. Scamarcio, M.S. Vitiello, H.E. Beere, D.A. Ritchie, THz quartz-enhanced photoacoustic sensor employing a quantum cascade laser source. In: M. Razeghi, E. Tournié, G.J. Brown (Eds.), Proceedings of SPIE - The International Society for Optical Engineering, vol. 8993, San Francisco, CA, USA, 2013, 89932O. https://doi.org/10.1117/12.2033620.
[22] A.A. Kosterev, Y.A. Bakhirkin, F.K. Tittel, Ultrasensitive gas detection by quartz-enhanced photoacoustic spectroscopy in the fundamental molecular absorption bands region, Appl. Phys. B 80 (2005) 133–138, https://doi.org/10.1007/s00340-004-1619-y.
[23] M. Mordmüller, M. Köhring, W. Schade, U. Willer, An electrically and optically cooperated QEPAS device for highly integrated gas sensors, Appl. Phys. B 119 (2015) 111–118, https://doi.org/10.1007/s00340-015-6037-9.
[24] P. Luo, J. Harrist, G. Menduni, R. Mesdour, N. StMichel, A. Sampaolo, Simultaneous detection of methane, ethane, and propane by QEPAS sensors for on-site hydrocarbon characterization and production monitoring, ACS Omega 7 (2022) 3395–3406, https://doi.org/10.1021/acsomega.1c05645.
[25] T. Liang, S. Qiao, Y. Chen, Y. He, Y. Ma, High-sensitivity methane detection based on QEPAS and H-QEPAS technologies combined with a self-designed 8.7 kHz quartz tuning fork, Photoacoustics 36 (2024) 100592, https://doi.org/10.1016/j.pacs.2024.100592.
[26] H. Wu, L. Dong, H. Zheng, Y. Yu, W. Ma, L. Zhang, W. Yin, L. Xiao, S. Jia, F. K. Tittel, Beat frequency quartz-enhanced photoacoustic spectroscopy for fast and calibration-free continuous trace-gas monitoring, Nat. Commun. 8 (2017) 15331, https://doi.org/10.1038/ncomms15331.
[27] M. Olivieri, G. Menduni, M. Giglio, A. Sampaolo, P. Patimisco, H. Wu, L. Dong, V. Spagnolo, Characterization of H2S QEPAS detection in methane-based gas leaks dispersed into environment, Photoacoustics 29 (2023) 100438, https://doi.org/10.1016/j.pacs.2022.100438.
[28] B. Li, C. Feng, H. Wu, S. Jia, L. Dong, Calibration-free mid-infrared exhaled breath sensor based on BF-QEPAS for real-time ammonia measurements at ppb level, Sens. Actuators B: Chem. 358 (2022) 131510, https://doi.org/10.1016/j.snb.2022.131510.
[29] B. Li, G. Menduni, M. Giglio, P. Patimisco, A. Sampaolo, A. Zifarelli, H. Wu, T. Wei, V. Spagnolo, L. Dong, Quartz-enhanced photoacoustic spectroscopy (QEPAS) and beat frequency-QEPAS techniques for air pollutants detection: a comparison in terms of sensitivity and acquisition time, Photoacoustics 31 (2023) 100479, https://doi.org/10.1016/j.pacs.2023.100479.
[30] W. Ye, W. Liu, W. Luo, J. Xiao, L. He, Y. Huang, D. Zhu, Calibration-free near-infrared methane sensor system based on BF-QEPAS, Infrared Phys. Technol. 133 (2023) 104784, https://doi.org/10.1016/j.infrared.2023.104784.
[31] F.O. Goodman, Application of a one-dimensional classical model of atom-oscillator scattering to atom-surface accommodation coefficient theory, Surf. Sci. 60 (1976) 45–64, https://doi.org/10.1016/0039-6028(76)90005-4.
[32] C. Lin, X. Yan, Y. Huang, An all-optical off-beam quartz-enhanced photoacoustic spectroscopy employing double-pass acoustic microresonators, Opt. Commun. 503 (2022) 127447, https://doi.org/10.1016/j.optcom.2021.127447.

Weilin Ye received her MS degree and PhD degree from the College of Electronic Science and Engineering, Jilin University, PR China, in 2009 and 2012, respectively. From 2016–2018, she worked as a post-doctoral fellow in the Electrical and Computer Engineering Department and Rice Quantum Institute, Rice University, Houston, USA. Now she is an associate professor in the College of Engineering, Shantou University, involved in the design, development and applications of infrared spectroscopy gas sensors.

Linfeng He received his B.E. degree in Design Manufacturing and Automation from Xihua University PR China, in 2021. He is pursuing a master's degree in mechanical engineering at Shantou University. His research interests include infrared spectroscopy , sensor technology.

Weihao Liu received his B.E. degree in Mechanical Design Manufacture and Automation from Shantou University, PR China, in 2021. He is now pursuing a master's degree in mechanical engineering at Shantou University. His research interests include system based on Arm-Linux, circuit design and control and laser spectroscopy.

Zhile Yuan received his B.E. degree in Mechanical Design Manufacturing and Automation from Shantou University, PR China, in 2024. He is pursuing a master's degree in mechanical engineering at Shantou University. His research interests include system based on photoacoustic spectroscopy.

Kaiyuan Zheng received his B.E. and Ph.D. degrees from Jilin University in 2016 and 2021, respectively. Following this, he served as a Postdoctoral Fellow at the Hong Kong Polytechnic University. He is currently a Research Assistant Professor at the Hong Kong University of Science and Technology. His research interests include optical fiber sensors, on-chip devices, and their environmental applications.

Guolin Li received the B.E. and Ph.D. degrees from Jilin University, Changchun, China, in 2010 and 2015, respectively. He is currently an Associate Professor and Doctoral supervisor with the China University of Petroleum (East China), Qingdao, China. His research interests include laser spectroscopy and intelligent photoelectric information processing.